Analyst

PAPER

View Article Online
View Journal | View Issue

Cite this: *Analyst*, 2017, **142**, 517

UiO-66@SiO_2 core–shell microparticles as stationary phases for the separation of small organic molecules†

R. D. Arrua,*[a,b] A. Peristyy,[a] P. N. Nesterenko,[a] A. Das,[c] D. M. D'Alessandro[c] and E. F. Hilder[a,b]

Received 25th October 2016,
Accepted 2nd January 2017

DOI: 10.1039/c6an02344d

www.rsc.org/analyst

Composite particles containing the Zr-based metal–organic framework (MOF) UiO-66 were prepared using microwave-assisted solvothermal synthesis. Scanning electron microscopy, infrared spectroscopy, powder X-ray diffraction and nitrogen physisorption studies confirmed the deposition of 100–300 nm microporous particles with the UiO-66 topology on the surface of mesoporous 5 μm and non-porous 2.1 μm silica particles. The core–shell particles exhibited a unique flow-dependent separation selectivity (FDSS) effect which allows changes in both the retention and separation selectivity of small molecules by simple variation of the mobile phase flow rate under isocratic conditions. The impact of the loading of UiO-66 as well as the porosity of the underlying silica core (mesoporous and non-porous) on the FDSS effect was evaluated. The prepared adsorbents were also tested for the normal-phase (NP) and reversed-phase (RP) separation of xylene isomers, substituted benzenes and polyaromatic hydrocarbons (PAHs). Efficiencies of up to 32 400 plates per m (styrene, *k* 1.59) and 37 200 plates per m (anisole, *k* 2.90) were achieved under NP and RP modes, respectively. The results demonstrate the potential of novel MOF-based stationary phases for the separation of closely related compounds (*e.g.* positional isomers).

1. Introduction

Metal–organic frameworks (MOFs) are highly ordered crystalline materials that are formed by linking metal-containing units (secondary building units) with organic linkers through the use of coordination bonds.[1] Since their invention, these materials have received considerable attention due to their tunable permanent porosity, their high surface areas and their potential for chemical functionalisation,[2] as well as the wide range of possible routes for their synthesis.[3] Owing to these highly advantageous characteristics, MOFs have been applied in gas storage,[4] heterogeneous catalysis[5] and for the separation of small molecules.[6] More recently, a number of research groups have sought to explore the application of these materials as stationary phases in liquid chromatography (LC).[6,7] To date, the MOF materials applied as stationary phases in LC include MOF-5,[8] HKUST-1,[8–12] MIL-47,[13,14] MIL-53(Al),[13–16] MIL-53(Fe),[17,18] MIL-101(Cr),[19,20] MIL-101(Fe),[21] ZIF-8,[22] chiral MOFs[23–25] and UiO-66.[26–31] The unique feature of MOFs as stationary phases (as compared with other separation media) is their capability to discriminate closely related compounds such as positional isomers (xylenes,[11,13,16–19,26,27,29–31] chloroanilines,[12,21] benzenediols,[15] chlorotoluenes,[18,19] dichlorobenzenes,[18,19] nitroanilines,[18] toluidines[21]) as well as polyaromatic hydrocarbons.[8,15,18] This unique selectivity has been attributed to a combination of molecular sieving and adsorption effects.

Early reports on the application of MOFs as stationary phases in LC used HPLC columns packed with MOF crystals.[8,13–21,23,25–28,30] A critical limitation in these packings involving nano/micro crystals was the high back pressure required for the mobile phase to flow through the small crystals, as well as the low efficiencies due to the inhomogeneous packing of crystals with irregular shapes.[9,22] With regards to the efficiencies of LC columns packed with MOFs, Liu *et al.*[15] reported efficiencies of up to 23 700 theoretical plates per m using MIL-53(Al) for the reversed-phase (RP) separation of various small molecules. Yang and Yan[19] achieved an efficiency of 20 000 plates per m (for the less retained ethylbenzene) under normal-phase (NP) separation conditions using only MIL-101(Cr) as a column packing. The same research group reported efficiencies of up to 13 000 plates per m for the separation of fullerenes[20] also using MIL-101(Cr).

In order to reduce the limitations associated with heterogeneous packings, composite silica/MOF stationary phases

[a]*Australian Centre for Research on Separation Science (ACROSS), School of Physical Sciences, University of Tasmania, Private Bag 75, Hobart 7001, Australia*
[b]*Future Industries Institute, University of South Australia, Mawson Lakes Campus, Mawson Lakes 5095, Australia. E-mail: Dario.Arrua@unisa.edu.au*
[c]*School of Chemistry F11, University of Sydney, NSW 2006, Australia*
†Electronic supplementary information (ESI) available. See DOI: 10.1039/c6an02344d

have also been prepared.[9,23,29] In this case, the MOF crystals were synthesised in the presence of silica particles and the resultant mixture (silica + MOFs) was packed within the LC column. Yan *et al.*[29] prepared silica-UiO-66 composite materials and used them in the NP separation of positional isomers and polyaromatic hydrocarbons (PAHs). The low efficiencies achieved (~5130–10 000 plates per m) using these composite materials were likely to arise from limitations due to band broadening due to the inhomogeneous packing of MOF crystals and silica particles with different shapes and sizes.

An alternate strategy towards the development of MOF-based stationary phases is the preparation of core–shell type silica/MOF composite particles.[11,22,31] This approach avoids the aforementioned limitations by synergistically combining the selectivity of the MOF-based shell and the favourable packing properties of the silica particles. Fu *et al.*[22] prepared SiO_2@ZIF-8 core–shell particles for the separation of endocrine disrupting chemicals and pesticides. The hybrid particles exhibited efficiencies of up to 23 000 plates per m.

Recently, our research group reported the microwave-assisted synthesis of UiO-66@SiO_2 core–shell particles which exhibited an unusual flow-dependent separation selectivity (FDSS) effect for the isocratic separation of small molecules.[32] We believe the FDSS effect would open new opportunities in the field of liquid chromatography by adding a new way of modifying the separation selectivity under isocratic conditions. The effect was observed for solutes in which the molecular sizes were comparable to the micropore size of the UiO-66 shell. UiO-66, $[Zr_6O_4(OH)_4(bdc)_6]$, is a MOF based on Zr(IV) ions and the organic linker 1,4-benzene dicarboxylate (bdc).[33] This framework has two types of microporous cavities (1.1 and 0.8 nm) which are accessible by 0.6 nm windows. The use of UiO-66 as a stationary phase is based on its well-known chemical, mechanical and thermal stability. In the current work, we analysed the impact of both the UiO-66 shell thickness and silica core porosity on the FDSS effect. The newly prepared particles were also tested for the NP and RP separation of xylene isomers, substituted benzenes and polyaromatic hydrocarbons (PAHs), achieving efficiencies that exceed the best values reported in the literature for the use of MOFs as stationary phases in LC.

2. Experimental

2.1 Materials and instrumentation

All the chemicals and instrumentation used in this work are detailed in the ESI.†

2.2 Synthesis of silica particles with bonded glutamic acid and UiO-66 crystals

The preparation of 5 μm silica particles containing bound glutamic acid functional groups (SiO_2(5)–COOH) and UiO-66 crystals was performed as previously described.[32]

2.3 Synthesis of UiO-66@SiO_2 core–shell particles

The deposition of UiO-66 nanocrystals on carboxylic acid-modified silica particles was performed following a similar procedure reported by our research group.[32] A 30 mL glass microwave vial was charged with 0.35 mg of modified silica particles (mesoporous 5 μm (SiO_2(5)–COOH) and commercially available non-porous 2.1 μm (SiO_2(2.1)–COOH) particles), 0.50 mmol $ZrCl_4$, 4 mL of concentrated HCl and 10 mL *N*,*N*′-dimethylformamide (DMF). The suspension was stirred for 30 min before 0.5 mmol of H_2bdc was added to the mixture. The suspension was placed within the microwave oven and heated with magnetic stirring to 160 °C within 30 min, and held at this temperature for 40 min before cooling to 55 °C within 1 min. The modified particles and UiO-66 nanocrystals were washed by centrifugation with portions of 20 mL DMF (6000 rpm, 3 times for 5 minutes) and 20 mL acetone (1000 rpm, 6 times for 1 minute). The washes with acetone at lower speeds allowed the separation of UiO-66 nanocrystals and the modified core–shell particles due to their difference in density. The resulting particles were dried under vacuum. A second deposition step of UiO-66 was performed onto the core–shell particles by following the same procedure as described above.

2.4 Packing procedure

All particles were packed within 50 × 2.1 mm ID stainless steel columns. The system for column packing consisted of a Haskel DSF-122 air driven liquid pump (Haskel International Inc., Burbank, CA, USA), which was connected in series to a 150 × 4.6 mm ID stainless steel slurry reservoir (volume 2.5 mL, purchased from Phenomenex, Lane Cove West, NSW, Australia), a 50 × 2.1 mm ID column extension and a 50 × 2.1 mm ID empty column with 0.5 μm pore size frits (all from Restek, Bellefonte, PA, USA). A slurry containing 0.10 g mL^{-1} of UiO-66@SiO_2 was prepared in DMF. The slurry concentration was chosen by considering a packing density of unmodified 5 μm Nucleosil (pore diameter 30 nm) of less than 1.1 g mL^{-1} with 25% excess used, with the volume of the reservoir being 2.5 mL. The empty column and column extension were filled with pure DMF in order to avoid bubbles, which may cause erratic slurry movements under the packing pressure. The slurry was placed in the reservoir, and 2-propanol was used as a pump fluid.

During the packing, the pump was operated manually, and the pressure program included a fast increase from 0 to 6000 psi within 3–5 seconds at the beginning of packing. Subsequently, the pressure was held at a target level of 6000 psi until ~100 mL of 2-propanol was pumped through the column. The pump was then turned off and after the pressure had decreased to 0 psi (within 2–3 min), the column was disconnected from the extension and the top frit and fitting were installed.

3. Results and discussion

3.1 Synthesis and characterisation of UiO-66@SiO_2 core shell particles

In order to study the effect of the porosity of the silica core on the deposition of MOFs, UiO-66 nanocrystals were deposited

onto the surface of COOH-modified mesoporous 5 μm (SiO_2(5)–COOH) and non-porous 2.1 μm (SiO_2(2.1)–COOH) silica particles. The deposition of UiO-66 was performed by microwave-assisted solvothermal synthesis.[34] This approach offers an easy and efficient synthesis of MOFs using shorter synthesis times than conventional solvothermal methods.[34,35] In this work, each deposition step of the UiO-66 crystals required less than 2 h. As a comparison, Zhang *et al.*[31] coated 5 μm amino-silica particles with UiO-66 nanocrystals using the conventional heating method. The authors performed the solvothermal deposition of UiO-66 crystals on the silica core using a total reaction time of 24 h. Therefore, the approach presented here is advantageous in terms of the reduction in synthesis time for the preparation of MOF-based stationary phases.

Fig. 1 shows SEM images of the 5 μm particles before and after one and two depositions of UiO-66 crystals. The uniform covering of 100–300 nm UiO-66 crystals on the surface of the SiO_2(5)–COOH particles is evident. As expected, the coating density of UiO-66 crystals is higher for the particles subjected to two deposition steps. Nitrogen adsorption–desorption isotherms for the unmodified SiO_2(5)–COOH particles and its composite derivatives with 1 and 2 deposition steps are shown in Fig. 2a. A transition is observed from a type I isotherm for the microporous UiO-66 crystals to a type IV isotherm for the UiO-66(1×)@SiO_2(5) and UiO-66(2×)@SiO_2(5) particles. The coating with UiO-66 crystals led to materials with higher

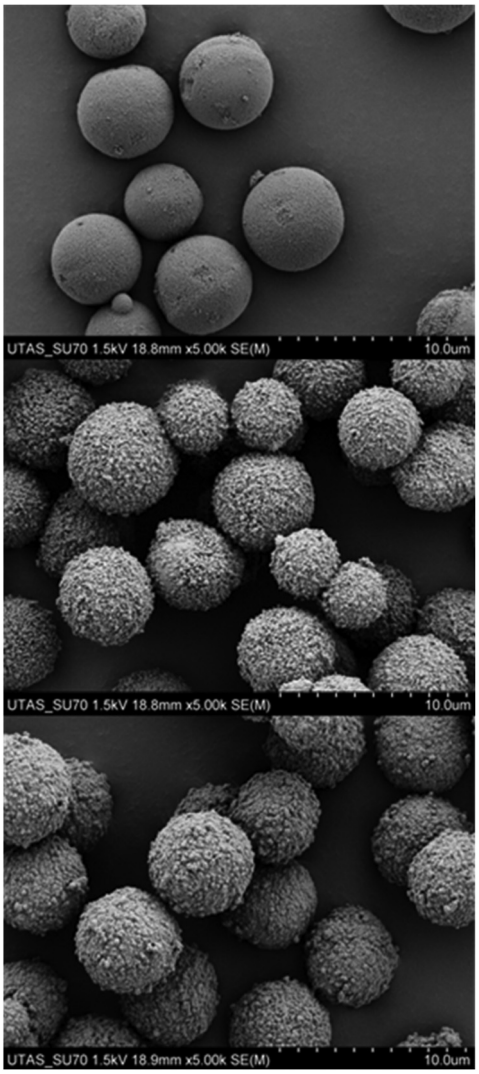

Fig. 1 Scanning electron microscopy images of SiO_2(5)–COOH (top), UiO-66(1×)@SiO_2(5) (middle) and UiO-66(2×)@SiO_2(5) (bottom) particles.

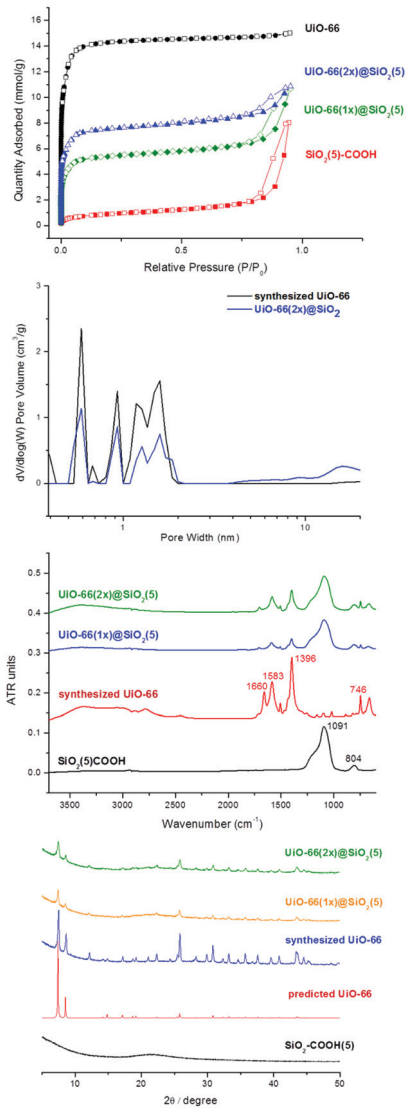

Fig. 2 (a) N_2 adsorption (filled) and desorption (open) isotherms at 77 K for SiO_2(5)–COOH (red squares), synthesized UiO-66 (black circles), UiO-66(1×)@SiO_2(5) (green diamonds) and UiO-66(2×)@SiO_2(5) (blue triangles) core–shell particles. (b) Pore size distribution curves obtained using the density functional theory (DFT) model for synthesized UiO-66 (black) and UiO-66(2×)@SiO_2(5) (blue) core–shell particles. (c) FT-IR spectra of SiO_2(5)–COOH (black), synthesized UiO-66 (red), UiO-66(1×)@SiO_2(5) (blue) and UiO-66(2×)@SiO_2(5) (green) core–shell particles. (d) PXRD patterns of SiO_2–COOH(5) (black), predicted UiO-66 (red), synthesized UiO-66 (blue), UiO-66(1×)@SiO_2(5) (orange) and UiO-66(2×)@SiO_2(5) core–shell particles (green).

Table 1 BET specific surface area and –COOH content of mesoporous SiO_2(5)–COOH, non-porous SiO_2(2.1)–COOH and various UiO-66@SiO_2 core–shell particles

Sample	BET S_s (m^2 g^{-1})	COOH content (μmol g^{-1})
UiO-66	1276.8	
SiO_2(5)–COOH	71.3	160[a]
UiO-66(1×)@SiO_2(5)	477.9	
UiO-66(2×)@SiO_2(5)	669.4	
SiO_2(2.1)–COOH	1.59	>30[b]
UiO-66(1×)@SiO_2(2.1)	136.3	
UiO-66(2×)@SiO_2(2.1)	479.4	

[a] Determined by elemental analysis. [b] As reported by the vendor.

specific surface areas (Table 1). For the 5 μm particles, surface areas increased from 71 m^2 g^{-1} for SiO_2(5)–COOH to 669 m^2 g^{-1} for the UiO-66(2×)@SiO_2(5) core–shell particles. Fig. 2b shows the pore size distribution curves of synthesised UiO-66 crystals and the core shell particles subjected to two deposition reactions. It is possible to see the well-defined microporous structure which is characteristic for the UiO-66 framework with pore sizes around 0.6, 0.8 and 1.1 nm. FT-IR and powder X-ray diffraction (PXRD) studies confirmed the presence of UiO-66 crystals in the prepared composite materials. FT-IR spectra for the prepared particles are shown in Fig. 2c. In all cases (except for the synthesised UiO-66 powder) peaks at around 1090 and 804 cm^{-1} can be observed, which correspond to the stretching vibration of Si–O and the bending vibration of SiO–H groups of the silica core, respectively. In the case of the core–shell particles, typical FTIR bands of the UiO-66 frameworks[33] were evident, with relatively higher intensity peaks recorded for the particles subjected to two deposition steps. The main peaks were observed at 1660 cm^{-1} (corresponding to DMF), 1583 and 1396 cm^{-1} (asymmetrical and symmetrical stretching bands of the carboxylate group respectively) and 746 cm^{-1} (C–H bending vibration of aromatic ring). PXRD (Fig. 2d) also confirmed the presence of particles with UiO-66 topology on the surface of the prepared UiO-66 (1×)@SiO_2(5) and UiO-66(2×)@SiO_2(5) microparticles.

Identical characterisation studies were conducted for the COOH-modified non-porous 2.1 μm particles (Fig. 1S and 2S in the ESI†). The analysis confirmed the deposition of UiO-66 crystals onto the surface of the smaller particles. However, the density of the UiO-66 framework covering the non-porous particles was lower than that obtained for the mesoporous 5 μm particles. This difference could be explained by considering the inherently lower BET surface area of the non-porous 2.1 μm particles (as compared with the mesoporous SiO_2(5)–COOH particles), as well as the lower specific amount of carboxylic acid groups available to build the UiO-66-based shell (Table 1). The results discussed above clearly show the rapid and successful coating of UiO-66 crystals on SiO_2 (mesoporous and non-porous) particles using the microwave-assisted synthesis protocol. Also, it was concluded that a thicker layer and higher density of UiO-66 crystals can be achieved for the mesoporous SiO_2(5)–COOH particles.

3.2 Evaluation of UiO-66@SiO_2 core shell particles as stationary phases

3.2.1 Flow-dependent separation selectivity. As shown in our preliminary work, the UiO-66@SiO_2 stationary phase exhibits a remarkable FDSS effect, where the separation selectivity of small organic molecules is dependent on the flow rate of a mobile phase of constant composition.[32] Accordingly, it was particularly interesting to investigate this effect for the series of adsorbents prepared in this work. Fig. 3S (ESI†) presents the selectivity–flow rate plots for different solutes. Clearly, for all MOF containing columns, the FDSS effect was observed. Furthermore, the largest variation in the selectivity *versus* flow rate was observed for the UiO-66(2×)@SiO_2(2.1) column. This is due to the fact that non-porous 2.1 μm silica has negligible surface area compared to the MOF (see Table 1), and thus does not contribute significantly to the retention of the solute. In contrast, increasing the number of deposited MOF layers, and thus the thickness of the MOF on the surface of the silica particles clearly leads to a larger variation in selectivity. In a similar fashion to the previously reported results from our group,[32] a decrease in the selectivity with the flow rate occurs for solutes with small sizes (toluene, ethyl benzene), while the separation selectivity of larger molecules like cumene and anthracene remains constant. Our hypothesis is that such behaviour is related to the slow kinetics of diffusion through the lattice of UiO-66 for the smaller molecules that can be accommodated, as confirmed by the plot for 5 μm SiO_2(5)–COOH column (Fig. 3S,† bottom left). For the latter column, the separation selectivity is independent of the flow rate for all compounds, which indicates that interactions between the solutes and the MOF arise due to the FDSS effect.

3.2.2 Normal phase separation of small organic molecules. The composite core–shell particles prepared were tested as stationary phases for the NP separation of a standard mixture of hydrocarbon compounds (Fig. 3). While the analytes tested could not be separated using the SiO_2(5)–COOH stationary phase (Fig. 4S†), all adsorbents decorated with UiO-66 particles showed a certain selectivity for the various analytes. This comparison clearly shows that the chromatograms observed arose from the presence of UiO-66 particles on the outer surface of the silica core.

As expected from the results discussed above regarding the characterisation of the core–shell particles, the UiO-66(1×)@SiO_2(2.1) phase containing the lowest amount of UiO-66 crystals only showed a small retention of *o*-xylene and naphthalene and almost no retention for the other analytes (Fig. 3c). The separation was considerably improved for the UiO-66(2×)@SiO_2(2.1) particles which were subjected to two depositions of UiO-66 particles (Fig. 3d). Improved results were observed for the composite phases obtained with the 5 μm mesoporous particles, with the best separation achieved for the column packed with UiO-66(2×)@SiO_2(5) particles (Fig. 3b). It can be seen that pentylbenzene and biphenyl are the least retained

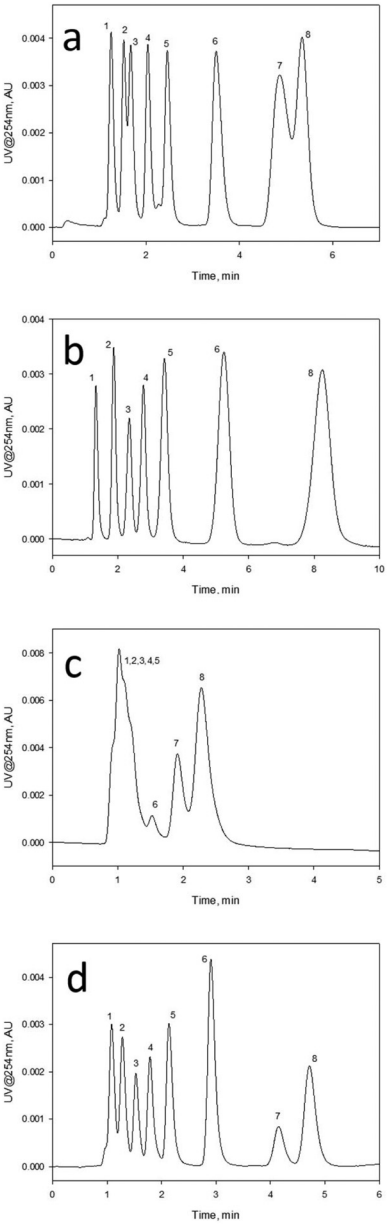

Fig. 3 Separation of a mixture of 7 or 8 hydrocarbons using 50 mm × 2.1 mm ID UiO-66@SiO_2 columns. Mobile phase – 0.2 ml min^{-1} of *n*-hexane, 25 °C, 2 μL injections of analytes (50 μg mL^{-1}) in mobile phase, UV detection at 254 nm. Analytes: 1 – pentyl benzene, 2 – biphenyl, 3 – ethyl benzene, 4 – styrene, 5 – *m*-xylene, 6 – phenyl acetylene, 7 – *o*-xylene, 8 – naphthalene. Columns: UiO-66(1×)@SiO_2(5) (a), UiO-66(2×)@SiO_2(5) (b), UiO-66(1×)@SiO_2(2.1) (c) and UiO-66(2×)@SiO_2(2.1) (d).

analytes of the series. This may be explained by considering the kinetic diameters of these analytes (0.687 and 0.666 nm for pentylbenzene and biphenyl, respectively) which prevents the analytes from entering the pores of the UiO-66 framework. Previously, we demonstrated[32] that organic molecules with diameters above ~0.63 nm could not penetrate the cavities of the framework and therefore they were weakly retained. It is also observed that styrene was more strongly retained than ethylbenzene. This selectivity has already been observed for other MOF-based stationary phases[8,11,19,29] and has been explained by considering the stronger π–π interactions between styrene and the bdc ligand, as well as coordinative interactions with the metal sites.[8] The same interactions would explain the stronger retention of phenyl acetylene and naphthalene. The higher retention observed for *o*-xylene relative to *m*-xylene can be attributed to the known reverse shape selectivity effect found for the UiO-66 framework.[26,27] In this case, bulkier analytes (*o*-xylene) approach the inner pore walls more closely and are retained strongly *via* van der Waals interactions. The reverse shape selectivity effect is also clearly observed in Fig. 4, which shows the separation of a standard mixture containing two types of positional isomers (*n*-propylbenzene and cumene) and xylene isomers. The bulkier cumene eluted after *n*-propylbenzene due to its stronger van der Waals interactions with the inner pore wall. The same effect also explains the elution order of xylenes, where the isomers eluted following the order *p*-xylene, *m*-xylene and *o*-xylene. The same elution order was previously reported for UiO-66-based stationary phases used in liquid[29,30] and gas chromatography.[36]

The UiO-66(2×)@SiO_2(5) core–shell particles were additionally tested for the separation of representative PAHs (Fig. 5). The retention times of the PAHs increased in the following order: benzene < anthracene < naphthalene ~ phenanthrene < pyrene. Such an elution order is different from that normally observed (*i.e.*, benzene < naphthalene < anthracene)[37,38] for common stationary phases (cyanopropyl- and alkyl amide phases with bonded polyaromatic moieties, *etc.*) and is consistent with retention by π–π stacking and hydrophobic inter-

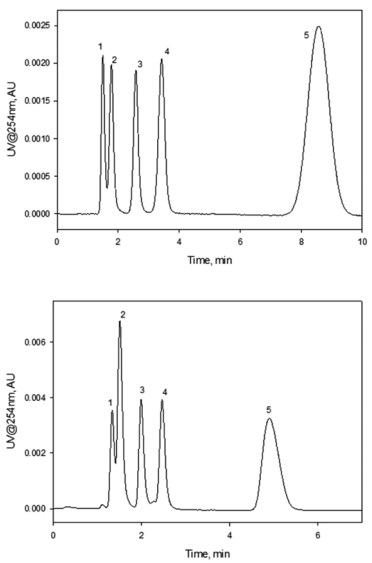

Fig. 4 Selectivity of UiO-66@SiO_2 stationary phases towards positional isomers. Mobile phase – 0.2 ml min^{-1} of *n*-hexane, 25 °C, 2 μL injections of analytes (50 μg mL^{-1}) in mobile phase, UV detection at 254 nm. Analytes: 1 – propyl benzene, 2 – cumene, 3 – *p*-xylene, 4 – *m*-xylene, 5 – *o*-xylene. Columns: UiO-66(2×)@SiO_2(5) (top) and UiO-66(1×)@SiO_2(5) (bottom).

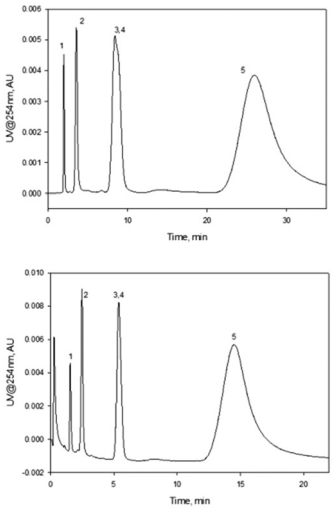

Fig. 5 Separation of a mixture of PAH with 50 mm × 2.1 mm ID UiO-66@SiO_2 columns. Mobile phase – 0.2 ml min^{-1} of *n*-hexane, 25 °C, 2 μL injections of analytes (50 μg mL^{-1}) in mobile phase, UV detection at 254 nm. Analytes: 1 – benzene, 2 – anthracene, 3 – phenanthrene, 4 – naphthalene, 5 – pyrene. Columns: UiO-66(2×)@SiO_2(5) (top) and UiO-66(1×)@SiO_2(5) (bottom).

actions. Generally, retention of PAHs gradually increases with the number of aromatic rings; the deviation from this rule in the current work can be explained by the contribution of additional retention mechanisms as mentioned above. Considering the FDSS effect and diffusion-regulated kinetics of adsorption, it would be reasonable to suggest a mixed mode retention mechanism of the PAH molecules on the UiO-66(2×)@SiO_2(5) phase with a combination of size-exclusion, hydrophobic and π–π interactions. Clearly, the kinetic diameter of the benzene molecule is smaller than the size of the pore window in UiO-66. Thus, it can freely diffuse within the MOF shell but does not interact strongly with the stationary phase, as it possesses only one aromatic ring. In contrast, naphthalene is still sufficiently small to penetrate the UiO-66 lattice, but interacts more strongly with the surface due to its fused π–π system. Furthermore, anthracene molecules having three aromatic rings are too large to penetrate the UiO-66 lattice, so they can interact only with the outer surface of the stationary phase; thus they are less strongly retained compared with naphthalene molecules of a smaller kinetic diameter. Surprisingly, phenanthrene is eluted significantly later than anthracene, despite their similar molecular sizes and structures. Considering the fact that the separation of anthracene and phenanthrene is usually a challenging task for common chromatographic columns,[38] such a separation selectivity of the UiO-66@SiO_2 stationary phase is remarkable and requires further investigation.

Table 2 shows the retention and column efficiency parameters calculated from the chromatogram shown in Fig. 3, obtained using the column packed with UiO-66(2×)@SiO_2(5) particles. The values are between 15 270–32 440 plates per m and they are close to or above the maximum efficiencies

Table 2 Peak parameters for the separation of hydrocarbons with UiO-66(2×)@SiO_2(5) particles under normal phase mode (see Fig. 3)

	Solute	t_R, min	k	Asymmetry @ 10%	N, plates per m
1.	Pentyl benzene	1.33	0.24	1.51	15 270
2.	Biphenyl	1.87	0.74	1.24	23 050
3.	Ethyl benzene	2.35	1.19	1.02	23 860
4.	Styrene	2.78	1.59	1.11	32 440
5.	*m*-Xylene	3.42	2.18	1.12	25 760
6.	Phenyl acetylene	5.24	3.87	1.01	20 800
8.	Naphthalene	8.25	6.67	0.93	24 020

reported in the literature for MOF-based stationary phases. As an example, the column efficiency for styrene (k = 1.59) was 32 440 plates per m, which is 6 times higher than 5130 plates per m obtained for the same analyte using a silica/UiO-66 composite stationary phase.[29] These results demonstrate the advantages of coating spherical particles with a shell of MOFs featuring a well-defined microporous structure.

3.2.3 Reversed phase separation of small organic molecules. The chromatographic behaviour of the prepared UiO-66@SiO_2 phase was also evaluated under RP conditions. Fig. 6 shows the isocratic separation of xylene isomers using a water–acetonitrile mixture (60 : 40, v/v) as a mobile phase. It can be seen that the bulkier *o*-xylene molecule has the longest elution time among the isomers. A similar effect was observed under NP conditions (see Fig. 4) which was explained based on the ability of *o*-xylene molecules to strongly interact with the inner pore walls of the framework (reverse shape selectivity).[26,27] However, the selectivity between *m*- and *p*-xylene is reversed to that observed under NP conditions. These results show the importance of the mobile phase in tuning the selectivity of MOF-based adsorbents, and demonstrate that the observed separations are a combination of size exclusion as well as non-covalent interactions (hydrophobic and π–π interactions) between the solutes and stationary phase. A similar separation selectivity was observed by Zhang and co-workers[31] who used related MOF-based core–shell particles in RP mode.

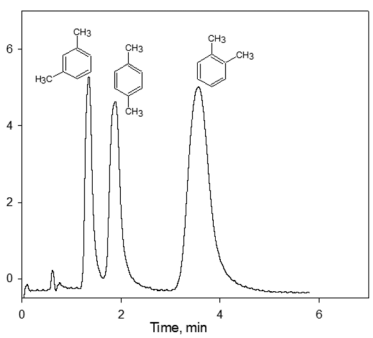

Fig. 6 Separation of the mixture of xylene isomers using UiO-66(1×)@SiO_2(5) column. Mobile phase – 40% ACN – 60% water, flow rate – 0.2 mL min^{-1}, 25 °C, UV detection at 254 nm, 2 μL injections of 50 μg mL^{-1} of analytes in mobile phase.

However, in the present work, the separation of xylene isomers was achieved in a significantly shorter time (less than 4 min) as compared with the 8 min needed in the previous report.[31]

The composite particles were also tested for the separation of 10 representative aromatic compounds under RP conditions (Fig. 7). It can be seen that baseline separation of 10 analytes could be achieved in less than 14 min using the UiO-66(1×)@SiO_2(5) (50 × 4.6 mm ID) column. In terms of efficiency (Table 3), N values from 7780 plates per m (for 2-methoxyphenol, k = 18.24) up to 37 220 plates per m (for anisole, k = 2.90) were achieved for the composite column showing the great potential of MOF-based phases for the separation of small molecules. In terms of selectivity, it should be noted again, that the UiO-66(1×)@SiO_2(5) phase exhibited significantly a stronger retention for the *ortho*-substituted compounds, *i.e.*, α(2-methoxyphenol/4-methoxyphenol) = 3.85. Generally, substituted phenols displayed surprisingly strong retention compared to what was expected for polar compounds in an acetonitrile–water (20 : 80 v/v) mobile phase. A simple explanation of this effect is based upon the H-bonding between the phenolic groups and $[Zr_6O_4(OH)_4]^{6-}$ clusters. This interaction observed for phenolic compounds could also explain the fact that compound 8 (4-ethylphenol) presented a wider peak than compound 9 (Toluene) despite of being less retained. It is known that H-bonding interactions can cause band broadening in RPLC.[39] Regarding the non-H-bonding solutes in Fig. 7, the elution time was generally shorter for the more polar molecules, in full agreement with the reversed phase principle. Overall, it can be concluded that UiO-66@SiO_2 is a mixed mode stationary phase, where the retention mechanism includes (but may not be limited to) hydrophobic interactions, π–π stacking and H-bonding. Indirectly, this fact can also be confirmed by the relatively poor efficiencies achieved for phenolic compounds in Table 3 (<12 000 plate per m), which is a clear indication of the multiple interactions that occur between the analytes and the stationary phase.

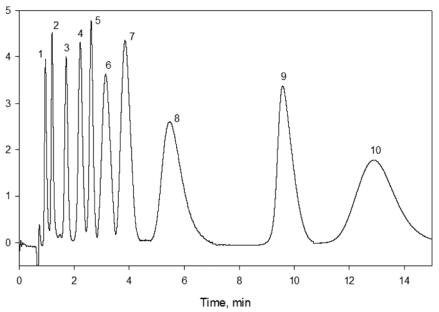

Fig. 7 Separation of 10 compounds using UiO-66(1×)@SiO_2(5) column. Mobile phase – 20% ACN – 80% water, flow rate – 0.2 mL min^{-1}, 25 °C, UV detection at 254 nm, 2 μL injections of 100 μg mL^{-1} of analytes in mobile phase. Analytes numbered as in Table 3.

Table 3 Peak parameters for the separation of hydrocarbons with UiO-66(1×)@SiO_2(5) particles under reversed phase mode (see Fig. 6)

	Solute	t_R, min	k	Asymmetry @ 10%	N, plates per m
1.	1,3,5-Trimethoxybenzene	0.95	0.41	1.23	16 160
2.	Methyl benzoate	1.19	0.78	1.26	25 800
3.	1,4-Dimethoxybenzene	1.70	1.54	1.07	20 680
4.	Biphenyl	2.21	2.30	1.10	20 080
5.	Anisole	2.61	2.90	1.08	37 220
6.	Phenol	3.14	3.68	1.11	9420
7.	4-Methoxyphenol	3.85	4.74	1.17	11 240
8.	4-Ethylphenol	5.48	7.18	1.42	5340
9.	Toluene	9.58	13.29	1.54	29 420
10.	2-Methoxyphenol	12.89	18.24	1.17	7780

4. Conclusions

Core shell particles decorated with UiO-66 were prepared by microwave-assisted solvothermal synthesis. The ease of preparation, short reaction time as well as the possibility of manufacturing quantitative amounts of modified particles makes the presented method a favourable alternative to currently used solvothermal approaches for the synthesis of similar MOF-based stationary phases. The deposition of UiO-66 was performed using mesoporous and non-porous silica particles, with a higher loading of UiO-66 material observed for the mesoporous counterpart. All the composite particles presented a unique FDSS effect, which was attributed to diffusion limitations of small molecules through the well-defined microporous skeleton of the UiO-66 layer. The particles were tested for the RP and NP separation of small molecules, and the highest efficiencies ever reported for MOF-based stationary phases were achieved. As reported for other MOF-based media, the different retention mechanisms of the tested analytes on the UiO-66@SiO_2 particles can be explained considering size-exclusion effects as well as hydrophobic, π–π and H-bonding interactions.

We hope the results presented in this work will encourage other scientists working in the field to develop similar core–shell particles decorated with MOFs possessing different pore shapes and sizes (micro/mesoporous). Clearly, further research should target the preparation of stable MOF-based composite adsorbents with improved core–shell structures, in order to achieve higher efficiencies. Further investigations are also needed to elucidate the unique selectivity of these phases, and to potentially identify niche applications in chromatography.

Acknowledgements

This work was supported by a Research Enhancement Grants Scheme (REGS), University of Tasmania and the Australian Research Council's Discovery funding scheme (DP130101471 and DP150101518).

Notes and references

1 H. Furukawa, K. E. Cordova, M. O'Keeffe and O. M. Yaghi, *Science*, 2013, **341**, 1230444–1230444.

2 D. Bradshaw, A. Garai and J. Huo, *Chem. Soc. Rev.*, 2012, **41**, 2344.
3 N. Stock and S. Biswas, *Chem. Rev.*, 2012, **112**, 933–969.
4 K. Sumida, D. L. Rogow, J. A. Mason, T. M. McDonald, E. D. Bloch, Z. R. Herm, T. H. Bae and J. R. Long, *Chem. Rev.*, 2012, **112**, 724–781.
5 M. Yoon, R. Srirambalaji and K. Kim, *Chem. Rev.*, 2012, **112**, 1196–1231.
6 J. R. Li, J. Sculley and H. C. Zhou, *Chem. Rev.*, 2012, **112**, 869–932.
7 Y. Yu, Y. Ren, W. Shen, H. Deng and Z. Gao, *Trends Anal. Chem.*, 2013, **50**, 33–41.
8 R. Ahmad, A. G. Wong-Foy and A. J. Matzger, *Langmuir*, 2009, **25**, 11977–11979.
9 R. Ameloot, A. Liekens, L. Alaerts, M. Maes, A. Galarneau, B. Coq, G. Desmet, B. F. Sels, J. F. M. Denayer and D. E. De Vos, *Eur. J. Inorg. Chem.*, 2010, **2010**, 3735–3738.
10 A. Ahmed, M. Forster, R. Clowes, P. Myers and H. Zhang, *Chem. Commun.*, 2014, **50**, 14314–14316.
11 A. Ahmed, M. Forster, R. Clowes, D. Bradshaw, P. Myers and H. F. Zhang, *J. Mater. Chem. A*, 2013, **1**, 3276–3286.
12 W. Qin, M. E. Silvestre, F. Kirschhofer, G. Brenner-Weiss and M. Franzreb, *J. Chromatogr., A*, 2015, **1411**, 77–83.
13 L. Alaerts, C. E. A. Kirschhock, M. Maes, M. A. van der Veen, V. Finsy, A. Depla, J. A. Martens, G. V. Baron, P. A. Jacobs, J. F. M. Denayer and D. E. De Vos, *Angew. Chem., Int. Ed.*, 2007, **46**, 4293–4297.
14 M. Maes, F. Vermoortele, L. Alaerts, S. Couck, C. E. A. Kirschhock, J. F. M. Denayer and D. E. De Vos, *J. Am. Chem. Soc.*, 2010, **132**, 15277–15285.
15 S. S. Liu, C. X. Yang, S. W. Wang and X. P. Yan, *Analyst*, 2012, **137**, 816–818.
16 W. De Malsche, S. Van der Perre, S. Silverans, M. Maes, D. E. De Vos, F. Lynen and J. F. M. Denayer, *Microporous Mesoporous Mater.*, 2012, **162**, 1–5.
17 R. El Osta, A. Carlin-Sinclair, N. Guillou, R. I. Walton, F. Vermoortele, M. Maes, D. de Vos and F. Millange, *Chem. Mater.*, 2012, **24**, 2781–2791.
18 Z. M. Yan, W. M. Zhang, J. Gao, Y. F. Lin, J. R. Li, Z. Lin and L. Zhang, *RSC Adv.*, 2015, **5**, 40094–40102.
19 C. X. Yang and X. P. Yan, *Anal. Chem.*, 2011, **83**, 7144–7150.
20 C. X. Yang, Y. J. Chen, H. F. Wang and X. P. Yan, *Chem. – Eur. J.*, 2011, **17**, 11734–11737.
21 Y.-Y. Fu, C.-X. Yang and X.-P. Yan, *J. Chromatogr., A*, 2013, **1274**, 137–144.
22 Y. Y. Fu, C. X. Yang and X. P. Yan, *Chem. – Eur. J.*, 2013, **19**, 13484–13491.
23 K. Tanaka, T. Muraoka, D. Hirayama and A. Ohnish, *Chem. Commun.*, 2012, **48**, 8577–8579.
24 D. Bradshaw, T. J. Prior, E. J. Cussen, J. B. Claridge and M. J. Rosseinsky, *J. Am. Chem. Soc.*, 2004, **126**, 6106–6114.
25 X. Kuang, Y. Ma, H. Su, J. Zhang, Y. B. Dong and B. Tang, *Anal. Chem.*, 2014, **86**, 1277–1281.
26 P. S. Barcia, D. Guimaraes, P. A. P. Mendes, J. A. C. Silva, V. Guillerm, H. Chevreau, C. Serre and A. E. Rodrigues, *Microporous Mesoporous Mater.*, 2011, **139**, 67–73.
27 M. A. Moreira, J. C. Santos, A. F. P. Ferreira, J. M. Loureiro, F. Ragon, P. Horcajada, K. E. Shim, Y. K. Hwang, U. H. Lee, J. S. Chang, C. Serre and A. E. Rodrigues, *Langmuir*, 2012, **28**, 5715–5723.
28 S. Van der Perre, T. Duerinck, P. Valvekens, D. E. De Vos, G. V. Baron and J. F. M. Denayer, *Microporous Mesoporous Mater.*, 2014, **189**, 216–221.
29 Z. M. Yan, J. N. Zheng, J. F. Chen, P. Tong, M. H. Lu, Z. Lin and L. Zhang, *J. Chromatogr., A*, 2014, **1366**, 45–53.
30 W. W. Zhao, C. Y. Zhang, Z. G. Yan, L. P. Bai, X. Wang, H. Huang, Y. Y. Zhou, Y. Xie, F. S. Li and J. R. Li, *J. Chromatogr., A*, 2014, **1370**, 121–128.
31 X. Zhang, Q. Han and M. Ding, *RSC Adv.*, 2015, **5**, 1043–1050.
32 A. Peristyy, P. N. Nesterenko, A. Das, D. M. D'Alessandro, E. F. Hilder and R. D. Arrua, *Chem. Commun.*, 2016, **52**, 5301–5304.
33 J. H. Cavka, S. Jakobsen, U. Olsbye, N. Guillou, C. Lamberti, S. Bordiga and K. P. Lillerud, *J. Am. Chem. Soc.*, 2008, **130**, 13850–13851.
34 W. Liang and D. M. D'Alessandro, *Chem. Commun.*, 2013, **49**, 3706–3708.
35 W. Liang, R. Babarao and D. M. D'Alessandro, *Inorg. Chem.*, 2013, **52**, 12878–12880.
36 N. Chang and X. P. Yan, *J. Chromatogr., A*, 2012, **1257**, 116–124.
37 J. Horak, N. M. Maier and W. Lindner, *J. Chromatogr., A*, 2004, **1045**, 43–58.
38 M. M. Rahman, M. Takafuji, H. R. Ansarian and H. Ihara, *Anal. Chem.*, 2005, **77**, 6671–6681.
39 J. Nawrocki, *J. Chromatogr., A*, 1997, **779**, 29–71.